Calculation of photodetachment cross sections and photoelectron angular distributions of negative ions using density functional theory

Yuan Liu and Chuangang Ning

Citation: The Journal of Chemical Physics **143**, 144310 (2015); doi: 10.1063/1.4932978
View online: http://dx.doi.org/10.1063/1.4932978
View Table of Contents: http://scitation.aip.org/content/aip/journal/jcp/143/14?ver=pdfcov
Published by the AIP Publishing

Calculation of photodetachment cross sections and photoelectron angular distributions of negative ions using density functional theory

Yuan Liu[1] and Chuangang Ning[1,2,a)]
[1]*Department of Physics, State Key Laboratory of Low-Dimensional Quantum Physics, Tsinghua University, Beijing 100084, China*
[2]*Collaborative Innovation Center of Quantum Matter, Beijing, China*

(Received 4 June 2015; accepted 29 September 2015; published online 13 October 2015)

Recently, the development of photoelectron velocity map imaging makes it much easier to obtain the photoelectron angular distributions (PADs) experimentally. However, explanations of PADs are only qualitative in most cases, and very limited works have been reported on how to calculate PAD of anions. In the present work, we report a method using the density-functional-theory Kohn-Sham orbitals to calculate the photodetachment cross sections and the anisotropy parameter β. The spherical average over all random molecular orientation is calculated analytically. A program which can handle both the Gaussian type orbital and the Slater type orbital has been coded. The testing calculations on Li^-, C^-, O^-, F^-, CH^-, OH^-, NH_2^-, O_2^-, and S_2^- show that our method is an efficient way to calculate the photodetachment cross section and anisotropy parameter β for anions, thus promising for large systems. © *2015 AIP Publishing LLC.* [http://dx.doi.org/10.1063/1.4932978]

I. INTRODUCTION

Photoelectron spectroscopy is a powerful tool for investigating the electronic structures of matters. The kinetic energy spectra and angular distributions of photoelectrons not only contain abundant information about the electronic states of atoms and molecules but also play an important role in photochemical dynamics. Compared with the fruitful information extracted from the photoelectron energy spectra, the exploration of the photoelectron angular distribution (PAD) is rather limited. Recently, the emergence[1] and development[2–5] of photoelectron velocity map imaging (VMI) technique makes it possible to measure the photoelectron energy spectra and angular distributions simultaneously without the need to rotate the electron energy analyzer. And lots of important works have been done by using it.[6–10] However, explanations to PADs are only qualitative in most cases, and rather limited works have been reported on how to calculate PAD of anions.[11–17]

The PAD is the differential cross sections of photoionization or photodetachment.[18–20] Yang's work[21] on the angular distribution in nuclear reactions in 1948 suggests that PADs for randomly oriented systems should take the general form of $1 + \alpha\cos^2\theta$, which is based only on the invariance properties of the physical process under space rotation and under inversion. Later, Cooper and Zare wrote PADs as the well-known form[15,16]

$$\frac{d\sigma}{d\Omega_k} = \frac{\sigma_{total}}{4\pi}[1 + \beta P_2(\cos\theta)]. \quad (1)$$

$P_2(\cos\theta)$ is the second-order Legendre polynomial, i.e., $(3\cos^2\theta - 1)/2$. The left side of Eq. (1) is the differential cross section, which is characterized by only two parameters in the right side. One is the total cross section σ_{total}, which is the integral of Eq. (1) over the full 4π solid angle, and the other is the so called anisotropy parameter β. Under certain photon energy for a specific bound state, these two parameters are the only measurable variables. In other words, they contain all the information that can be known in such processes.

By combining the Wigner threshold law[22] and the well-established partial-wave scattering theory, the experimental values of anisotropy parameter β can be qualitatively understood. However, how to calculate β accurately is nontrivial. Many methods have been proposed. Bethe and coworkers derived,[23] and later generalized by Cooper and Zare,[16] that the anisotropy parameter β under electric-dipole approximation for photoemission using linearly polarized light can be described by the Cooper-Zare equation, which assumes that the initial bound states can be described by a definite angular momentum value, and thus is usually only suitable for atomic cases. Besides, the Cooper-Zare equation contains integrals for calculating the radial transition matrix, which is a barrier for using the formula. Later, Hanstorp *et al.* simplified the Cooper-Zare equation by substituting the radial transition matrix integral with relative scaling of partial-wave cross sections that is proportional to the kinetic energy of the emitted electron according to the Wigner threshold law.[13] However, as in most cases, instead of possessing only one definite angular momentum value, the molecular orbitals (MOs) are usually hybridizations of many atomic orbitals with different angular momentum values; thus, Cooper-Zare equation is not applicable any more at such circumstances. Then, the mixed s-p state model is proposed by Grumbling and Sanov to overcome this problem.[14] This model regards the detached bound state as a linear combination of one s orbital with a fraction of $(1 - f)$ and one p orbital with a fraction of f localized on the same center in a molecule, where f is the fractional p-character of the state and satisfies $0 \le f \le 1$.

a)Electronic mail: ningcg@tsinghua.edu.cn

The mixed s-p state model has successfully predicted how β depends on the kinetic energy of the detached electron in many systems including polyatomic anions.[11,24,25] Although this model is, on its surface, analytical and simple to use, however, as Sanov[12] has pointed out that parameters such as the p fractional character f and the effective nuclear charge ζ have to be determined by *ab initio* calculations of the corresponding MOs. And its serious drawback lies on the central-atom approximation. To interpret the time-resolved photoelectron imaging spectra of neutral polyatomic molecules, Mitric and coworkers reported an efficient method based on the time-dependent density functional theory (TD-DFT).[26] Recently, Krylov and coworkers reported a wave-function-based method using the Dyson orbitals from equation-of-motion coupled-cluster (EOM-CC) theory[27–29] to calculate photodetachment cross sections and PADs of anions.[30,31] It should be noted that the computational cost of the sophisticated coupled-cluster calculation is very high for a large system, especially for anions whose diffuse nature of wave functions needs to be described by large basis sets.[30]

Both theoretical and experimental efforts have shown that the Kohn-Sham orbitals[32,33] obtained using density functional theory (DFT) are very a good approximation to the Dyson orbitals, especially for valence orbitals,[32,34–37] as will be demonstrated in Section IV A. Here, we report a method to calculate the photodetachment cross sections and PADs of anions using the DFT Kohn-Sham orbitals. The spherical average over all orientation of anions is realized analytically. The testing calculations on Li^-, C^-, O^-, F^-, CH^-, OH^-, NH_2^-, O_2^-, and S_2^- anions have been conducted using different Gaussian type orbitals (GTOs) and Slater type orbitals (STOs). The comparison between the calculated results and experimental data suggests that our method provides an efficient way to calculate the photodetachment cross section and the anisotropy parameter β of anions without losing accuracy and reliability, and is promising to be widely used, especially for large systems.

II. THEORY

The differential cross section for detaching an electron under electric dipole approximation is (in atomic units)[23]

$$\frac{d\sigma}{d\Omega_k} = \frac{4\pi^2 E}{c}\left|M_k^{fi}(\theta_k,\varphi_k)\right|^2, \tag{2}$$

where E is the photon energy for detachment, c is the velocity of light in vacuum, the subscript k indicates the outgoing electron's wave vector. $M_k^{fi}(\theta_k,\varphi_k)$ is the electric dipole transition matrix,

$$M_k^{fi}(\theta_k,\varphi_k) = \left\langle \Psi_F^{N-1}\Psi_k \left|\vec{\varepsilon}\cdot\vec{r}\right| \Psi_I^N \right\rangle. \tag{3}$$

Furthermore, Ψ_I^N and Ψ_{F}^{N-1} are the total wave functions of the initial N electron system and the remaining $N-1$ electron core, respectively. Ψ_k stands for the outgoing electron, which can be described by a plane wave $e^{i\vec{k}\cdot\vec{r}}$. $\langle\Psi_F^{N-1}|\Psi_I^N\rangle$ is called Dyson orbital. If the total wave functions of the system are constructed using DFT, with the frozen orbital approximation, Eq. (3) can be simplified as

$$M_k^{fi}(\theta_k,\varphi_k) = \int \Psi_k(\vec{\mathrm{r}})\mathrm{z}\phi_i^{KS}(\vec{\mathrm{r}}')d\tau', \tag{4}$$

where $\phi_i^{KS}(\vec{\mathrm{r}}')$ is the Kohn-Sham orbital from which the electron is detached[33] and $\vec{\mathrm{r}}'$ is displacement vector of the electron in the molecular-frame (M-frame). For convenience, the variables in M-frame are decorated with a prime, and those in the laboratory-frame without it. $\vec{\varepsilon}$ is the polarization of the incident light, which, without loss of generality, has been set along the z axis in L-frame, and $d\tau'$ is the integration volume unit in M-frame. The M-frame is fixed on the molecule, while the L-frame is fixed on the laboratory.

For randomly oriented gas phase anions, the average of electric dipole transition matrix over all directions is required.[38] In order to do this, we make the M-frame and the L-frame have the same coordinate origin, which lies on the center of the detached orbital. Then, the rotation of gas phase molecules in 3-dimension space is represented by the relative orientation between the M-frame and L-frame, which is further characterized by the Euler angles α, β, and γ between these two frames. Thus, the average is

$$\overline{\left|M_k^{fi}(\theta_k,\varphi_k)\right|^2} = \frac{1}{8\pi^2}\int d\alpha d\beta d\gamma \sin\beta \left|M_k^{fi}(\theta_k,\varphi_k)\right|^2. \tag{5}$$

For 1-electron detachment process of anions, a neutral core will be left. The interaction between the detached electron and the left neutral core is very weak. Therefore, the outgoing electron can be described by a plane wave

$$\Psi_k(\vec{\mathrm{r}}) = \sqrt{\frac{k}{(2\pi)^3}}e^{i\vec{k}\cdot\vec{r}}, \tag{6a}$$

where we have normalized the plane wave per unit energy.[23] k is the wave vector of the outgoing electron, given by (in atomic units)

$$k = \sqrt{2(E-E_b)}, \tag{6b}$$

where E_b is the binding energy of the detached electron.

It has been shown that orthogonality between the plane wave and Kohn-Sham orbital is important for reproducing the threshold behavior of the cross sections.[39] So here we impose the orthogonality relation by placing the coordinate origin of L-frame in the centroid of the Kohn-Sham orbitals.[30] In order to calculate the integral in Eq. (5) in M-frame first and then average over all the Euler angles, we employ the plane wave expansion in M-frame,

$$e^{i\vec{k}\cdot\vec{r}} = 4\pi\sum_{l=0}^{\infty}\sum_{m=-l}^{l} i^l j_l(\mathrm{k'r'})\mathrm{Y}_{lm}(\theta',\varphi')\mathrm{Y}_{lm}^*(\theta_k',\varphi_k'), \tag{7}$$

where Y_{lm} is the spherical harmonics, j_l the spherical Bessel function, and the asterisk indicates a complex conjugate. As L-frame and M-frame have common origin, $k = k'$ and $r = r'$. Now since the differential cross section is measured in L-frame, we need to transform $Y_{lm}^*(\theta_k',\varphi_k')$ in Eq. (7) from M-

frame to L-frame, which is

$$Y^*_{lm}(\theta'_k,\varphi'_k) = \sum_{m_1=-l}^{l} D^{*l}_{m_1,m}(\alpha,\beta,\gamma)Y^*_{lm_1}(\theta_k,\varphi_k), \quad (8)$$

where $D^l_{m_1,m}(\alpha,\beta,\gamma)$ is the 3-d rotation matrix, as defined by Rose.[40] We can also write the electric dipole operator z in spherical harmonics and evoke the inverse transform of Eq. (8) to get

$$\begin{aligned} z &= (\frac{4\pi}{3})^{\frac{1}{2}} rY_{10}(\theta,\varphi) \\ &= (\frac{4\pi}{3})^{\frac{1}{2}} r \sum_{m_2=-1}^{1} D^{*1}_{0,m_2}(\alpha,\beta,\gamma)Y_{1,m_2}(\theta',\varphi'). \end{aligned} \quad (9)$$

Combining Eqs. (2)–(9), we obtain the differential cross section

$$\begin{aligned} \frac{d\sigma}{d\Omega_k} &= \frac{kE}{3c}\int d\alpha d\beta d\gamma \sin\beta \left| \sum_{l=0}^{\infty}\sum_{m=-l}^{l}\sum_{m_1=-l}^{l}\sum_{m_2=-1}^{1} \Theta_{klmm_2} D^{*l}_{m_1m}(\alpha,\beta,\gamma) D^{*1}_{0m_2}(\alpha,\beta,\gamma) Y^*_{lm_1}(\theta_k,\varphi_k) \right|^2 \\ &= \frac{kE}{3c}\int d\alpha d\beta d\gamma \sin\beta \sum_{lmm_1m_2}\sum_{l'm'm_1'm_2'} \Theta_{klmm_2}\Theta^*_{kl'm'm_2'} D^{*l}_{m_1m} D^{*1}_{0m_2} D^{l'}_{m_1'm'} D^{1}_{0m_2'} Y^*_{lm_1} Y_{l'm_1'}, \end{aligned} \quad (10)$$

where

$$\begin{aligned} \Theta_{klmm_2} = \int & i^l j_l(\mathrm{k'r'}) \mathrm{Y}_{lm}(\theta',\varphi') \mathrm{Y}_{1m_2}(\theta',\varphi') \phi^{KS}_i(\vec{\mathrm{r}}') \\ & \times \mathrm{r'}^3 \sin\theta' d\mathrm{r}' d\theta' d\varphi' \end{aligned} \quad (11)$$

is an integral in M-frame and does not depend on Euler angles. For the simplicity of notation, we have omitted the arguments of rotation matrix and spherical harmonics in the second line of Eq. (10). The integral in Eq. (10) over Euler angles can be calculated analytically by using Clebsch-Gordan series

$$\begin{aligned} & D^{l_1}_{m_1\mu_1}(\alpha,\beta,\gamma) D^{l_2}_{m_2\mu_2}(\alpha,\beta,\gamma) \\ &= \sum_{j=|l_1-l_2|}^{l_1+l_2} C(l_1l_2j;m_1m_2)C(l_1l_2j;\mu_1\mu_2) \\ & \times D^j_{m_1+m_2,\mu_1+\mu_2}(\alpha,\beta,\gamma), \end{aligned} \quad (12)$$

where $C(l_1l_2j;m_1m_2)$ is the Clebsch-Gordan coefficient, as defined by Rose.[40] Substitute Eq. (12) into Eq. (10) and then use the orthonormal relation of rotation matrix

$$\begin{aligned} & \int d\alpha d\beta d\gamma \sin\beta D^{*L}_{m\mu}(\alpha,\beta,\gamma) D^{L'}_{m'\mu'}(\alpha,\beta,\gamma) \\ &= \frac{8\pi^2}{2L+1}\delta_{LL'}\delta_{mm'}\delta_{\mu\mu'}, \end{aligned} \quad (13)$$

and it yields

$$\begin{aligned} \frac{d\sigma}{d\Omega_k} = & \frac{kE}{3c} \sum_{lmm_1m_2}\sum_{l'm'm_1'm_2'} \Theta_{klmm_2}\Theta^*_{kl'm'm_2'} Y^*_{lm_1}(\theta_k,\varphi_k) \\ & \times Y_{l'm_1'}(\theta_k,\varphi_k) \sum_{L=|l-1|}^{l+1}\sum_{L'=|l'-1|}^{l'+1} C^*(l1L;m_10) \\ & \times C^*(l1L;mm_2)\cdot C(l'1L';m_1'0)C^*(l'1L';m'm_2') \\ & \times \frac{8\pi^2}{2L+1}\delta_{LL'}\delta_{m_1m_1'}\delta_{m+m_2,m'+m_2'}. \end{aligned} \quad (14)$$

Equation (14) is the final explicit expression for differential cross section measured in the L-frame. From it, we can easily calculate the anisotropy parameter β and total detachment cross section of anions.

If we set $\theta = 0(\parallel)$ and $\frac{\pi}{2}(\perp)$ in Eq. (1) separately, then the total cross section σ_{total} and anisotropy parameter β are given by

$$\sigma_{total} = \frac{4\pi}{3}\left(\frac{d\sigma}{d\Omega_{k\,\parallel}} + 2\frac{d\sigma}{d\Omega_{k\,\perp}}\right) \quad (15a)$$

and

$$\beta = 2\left(\frac{d\sigma}{d\Omega_{k\,\parallel}} - \frac{d\sigma}{d\Omega_{k\,\perp}}\right)/\left(\frac{d\sigma}{d\Omega_{k\,\parallel}} + 2\frac{d\sigma}{d\Omega_{k\,\perp}}\right). \quad (15b)$$

TABLE I. Electron affinities and states used in the calculations.

Anion	Electron affinity (eV)	States (M ← M⁻)	Factor	References
Li^-	0.618	$(2s)\,^2S_{1/2} \leftarrow (2s^2)\,^1S_0$	1	52 and 53
C^-	1.260	$(2p^2)\,^3P_0 \leftarrow (2p^3)\,^4S_{3/2}$	1.5	54
O^-	1.460	$(2p^4)\,^3P_2 \leftarrow (2p^5)\,^2P_{3/2}$	2	55
F^-	3.400	$(2p^5)\,^2P_{3/2} \leftarrow (2p^6)\,^1S_0$	3	56 and 57
CH^-	1.238	$^2\Pi \leftarrow {}^3\Sigma^-$	1	58
OH^-	1.830	$^2\Pi \leftarrow {}^1\Sigma^+$	2	59
NH_2^-	0.744	$^2B_1 \leftarrow {}^1A_1$	1	60
O_2^-	0.448	$^3\Sigma_g^- \leftarrow {}^2\Pi_g$	1	61
S_2^-	1.670	$^3\Sigma_g^- \leftarrow {}^2\Pi_g$	1	62

For cases where degeneracy exists, the cross section results need to be multiplied by the degeneracy factors. The factors for the anions in the present work are listed in Table I.

III. COMPUTATION DETAILS

We have coded a program in FORTRAN language using DFT Kohn-Sham orbitals to calculate the photodetachment cross section and the anisotropy parameter β for the randomly oriented anions in gas phase. The spherical average over all random orientation is done analytically. Several atomic and molecular anions including Li^-, C^-, O^-, F^-, CH^-, OH^-, NH_2^-, O_2^-, and S_2^- are investigated. Both the STO and the GTO are supported by our program now.

The Kohn-Sham orbitals are generated using the hybrid B3LYP (Becke, three-parameter, Lee-Yang-Parr)[41–43] functional with GAUSSIAN[44] and ADF packages.[45] The geometries of those anions have been optimized at the same level. Since the wave function of anions is very diffuse, the large basis sets are necessary to obtain the accurate description of the valence orbitals. To examine the basis sets dependency, for STO basis sets, we employ QZ3P-nd (n = 1, 2, even tempered valence quadruple zeta basis sets plus three polarization functions and *n* diffuse sets of s, p, d, f functions), while for GTO basis sets, Dunning's correlation-consistent basis sets[46] aug-cc-pVnZ (AVnZ, n = T, Q, 5, 6, as the usual definition) are used. Electron affinity (EA) values used in our calculation are taken from the previous experiments, as shown in Table I.

The electron momentum spectroscopy (EMS), based on the kinetically complete (e, 2e) experimental, is another important tool for investigating the electronic structures of atoms and molecules.[47,48] It can measure the electron density distribution in the momentum space for each molecular orbital. The density distributions of Dyson orbitals and Kohn-Sham orbitals have been extensively compared in the momentum space. It has been found that Dyson orbitals can be well approximated by Kohn-Sham orbitals for the molecular valence orbitals.[32,34–37] Here, the spherically averaged electron momentum distributions of Dyson orbitals and Kohn-Sham orbitals of Ne, H_2O, NH_3, and CH_4 are in comparison with the experimental distributions for enhancing and demonstrating this conclusion. The experimental momentum density distributions were measured using our high resolution electron momentum spectrometer at the electron impact energy 1200 eV.[49,50] More details can be found in our previous report.[34] Dyson orbitals are generated using the high level symmetry-adapted-cluster (SAC) configuration-interaction (CI) theory.[34,51] The AVTZ basis sets for Ne, H_2O, NH_3, CH_4, F^-, and Li^- are used. The R^- operators up to quadruple are included. The active space includes full molecular orbitals. Perturbation selections are conducted to reduce the computation time. The threshold of the linked terms for the ground state is 1.0×10^{-6}, and the unlinked terms are included as the products of the linked terms whose single- and double-configuration-interaction (SDCI) coefficients are larger than 5.0×10^{-3}. Kohn-Sham orbitals are calculated at B3LYP/AVQZ level of theory. Both are calculated using GAUSSIAN package.[44] The theoretical electron momentum distributions are then generated using a home-coded program *NEMS*.[37]

IV. RESULTS AND DISCUSSION

A. Comparison of Dyson orbitals and Kohn-Sham orbitals

Fig. 1 shows the spherically averaged electron momentum distributions of the highest occupied molecular orbitals (HOMOs) of Ne, H_2O, NH_3, and CH_4 calculated using Dyson orbitals and Kohn-Sham orbitals. The experimental distributions of H_2O, NH_3, and CH_4 are from our previous work.[34] For 2p orbital of Ne and $1t_2$ orbital of CH_4, Dyson orbital (red line) and Kohn-Sham orbital (blue line) produce nearly the same electron momentum distributions, and both are in excellent agreement with the experimental distributions. For $1b_1$ orbital of H_2O and $3a_1$ orbital of NH_3, both Dyson orbital

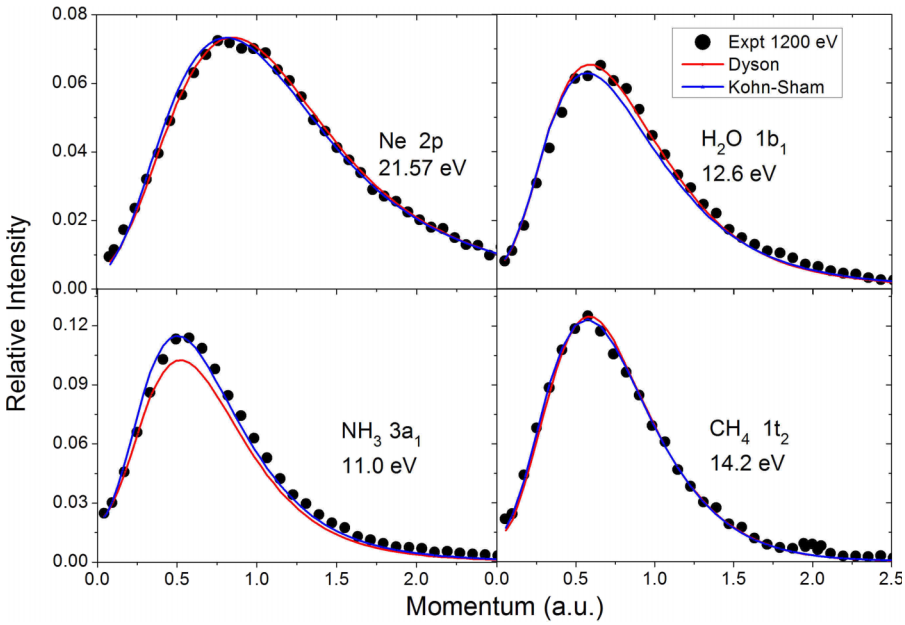

FIG. 1. Spherically averaged electron momentum distributions of HOMOs of Ne, H_2O, NH_3, and CH_4. The binding energies and orbital labels for the orbitals are listed in each panel.

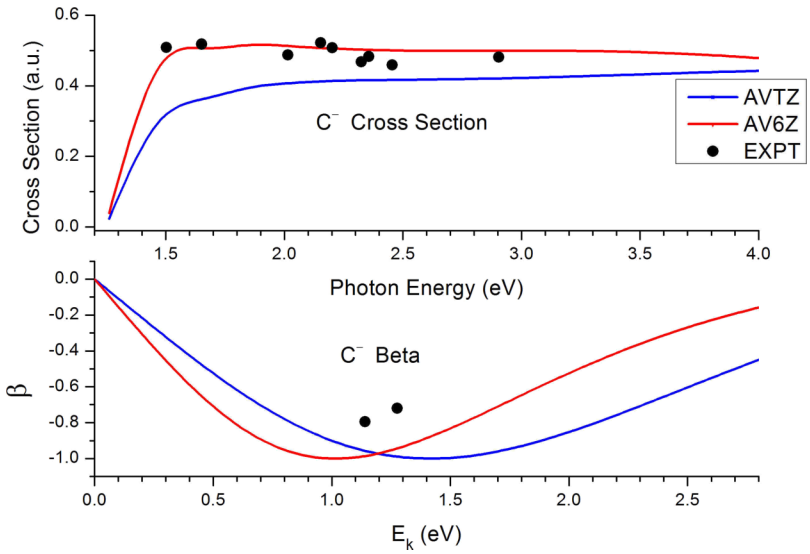

FIG. 2. Calculated photodetachment cross section (upper panel) and anisotropy parameter β (lower panel) of C^- anion with AVTZ (in blue) and AV6Z (in red) basis sets. The experimental data (black circle) are from Refs. 63 and 64.

and Kohn-Sham orbital agree well with the experimental results except the slightly different maximum intensities. Generally, Dyson orbitals can be well approximated by the Kohn-Sham orbitals.

B. Photodetachment cross sections and anisotropy parameters

Fig. 2 shows the total photodetachment cross section (upper panel) and anisotropy parameter β of photoelectron angular distribution (lower panel) of C^- calculated using AVTZ (aug-cc-pVTZ, blue line) and AV6Z (aug-cc-pV6Z, red line) basis sets, compared with experimental data[63,64] (black circle). E_k is the kinetic energy of the outgoing electron. It can be seen that AV6Z basis sets well reproduce the experimental cross section, while AVTZ basis sets slightly underestimate the cross section and give a slow rise near the threshold photon energy. In the lower panel, both of them give a right trend of β values, except for the slight underestimation. Again, AVTZ behaves a little bit worse than AV6Z. At the energy threshold ($E_k = 0$), as expected, both basis sets predict $\beta = 0$, since HOMO of C^- is a p orbital and the outgoing electron is (s + d) wave. When $E_k = 0$, d wave is highly suppressed, and only s wave left, which corresponds to $\beta = 0$. As the photon energy increases, the contribution from d wave increases, so β gradually decreases. When s wave and d wave have equal contributions, β goes down to -1. As the energy continues to increase, d wave becomes dominant, β begins to increase again. The calculation well reproduces this behavior. It is a pity that there are only two points of experimental β data.

Fig. 3 shows the calculated photodetachment cross section (upper panel) and anisotropy parameter (lower panel) β of O^-. Experimental data (black and open circle) are from Refs. 13, 65, and 66. HOMO of O^- anion is also a p orbital, so it should behave generally in the same way as C^-. Indeed, it is the case as shown in Fig. 3. In the upper panel of Fig. 3, all calculations tend to underestimate the cross section, but the overall trend agrees with the experimental results very well. The calculation based on the STO basis set QZ3P-1d produces almost the same results as the GTO basis set AV6Z. In the lower panel, the calculations overestimate β in the low energy region and underestimate it in the high energy region. In other

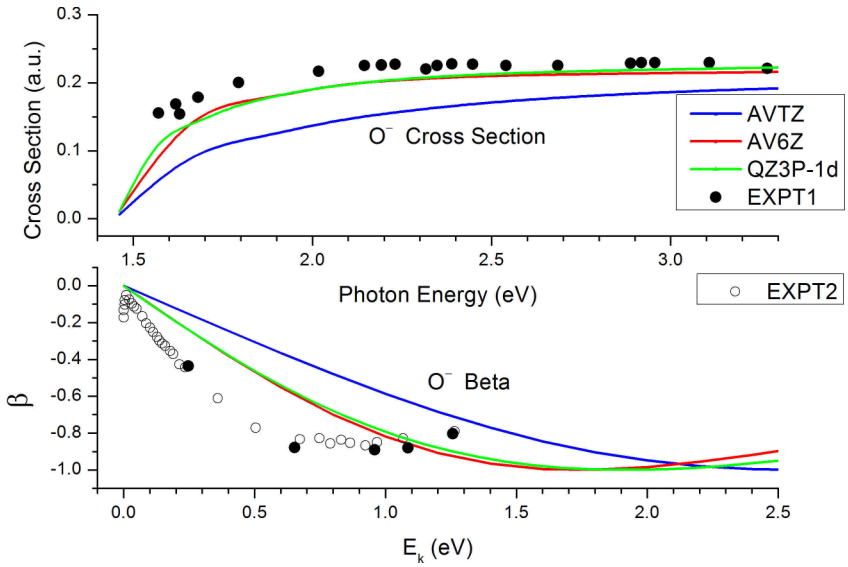

FIG. 3. Calculated photodetachment cross section (upper panel) and anisotropy parameter β (lower panel) of O^- anion with AVTZ (in blue), AV6Z (in red), and STO QZ3P-2d (in green) basis sets. The experimental data EXPT1 (black circle) are from Refs. 13 and 65, EXPT2 (open circle) from Ref. 66.

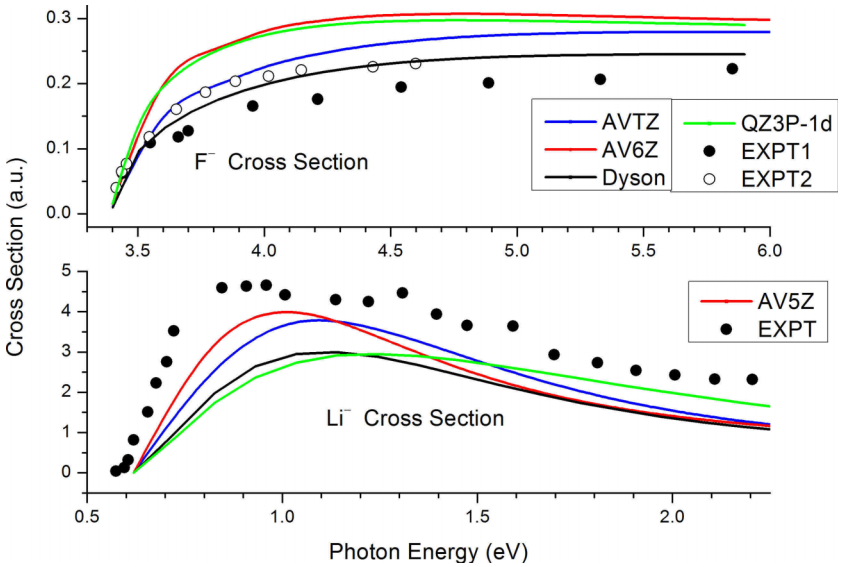

FIG. 4. Calculated photodetachment cross section of F^- anion (upper panel) and Li^- anion (lower panel) with AVTZ (in blue), AV5Z, and AV6Z (both in red), and STO QZ3P-2d (in green) basis sets with DFT methods. The calculated results using Dyson orbitals with the SAC-CI/AVTZ method are in black. The experimental data (black circle, F^-) are from Refs. 67 and 68 (open circle, F^-), and Ref. 69 (black circle, Li^-).

words, the calculations change slower than experimental β values as the photon energy increases.

Fig. 4 shows the photodetachment cross section of F^- (upper panel) and Li^- (lower panel). HOMO of F^- is also a p orbital. Therefore, a similar behavior as for C^- and O^- is observed. The calculations with basis sets AV6Z and QZ3P-1d slightly overestimate the cross section compared to the experimental data,[67] while the trend is correct. The calculation based on the Dyson orbital with the AVTZ basis set is similar to that on the DFT Kohn-Sham orbital in shape. The SAC-CI calculation predicts that its normalization constant, the spectroscopic factor, is 0.85, less than the normalization for DFT Kohn-Sham orbital (one). Therefore, the calculated cross section is lower than the DFT result. It agrees well with the experimental data from Ref. 68 and is slightly higher than the experimental data from Ref. 67. For Li^- anion, the electron is photodetached from a 2s orbital. Therefore, the outgoing electron should be a pure p wave. Our calculation indeed gives $\beta = 2$ for all photon energies (not illustrated here). Since AV6Z basis sets are not supported for Li, AV5Z is instead used here. Both AVTZ and AV5Z slightly underestimate the cross section (~10%), but the overall profiles are good. Again, the calculation based on the Dyson orbital with the AVTZ basis set is similar in shape to that on the DFT Kohn-Sham orbital with the same basis set. The SAC-CI calculation predicted a spectroscopic factor 0.78, which is due to the correlation in the initial state Li^- because the final state Li has no valence correlation in its $1s^22s$ configuration. Thus, the calculated cross section is lower than the DFT prediction. The calculation STO basis set for Li^- significantly underestimates the experimental cross section as the photon energy less than 1.7 eV. The agreement improves for the higher photon energy.

The above examples show that our method can well describe the detachment cross section and anisotropy parameter β of atomic anions. To further test our method, several molecular anions are also investigated.

Figs. 5 and 6 show the photodetachment cross section (upper panel) and anisotropy parameter β (lower panel) of

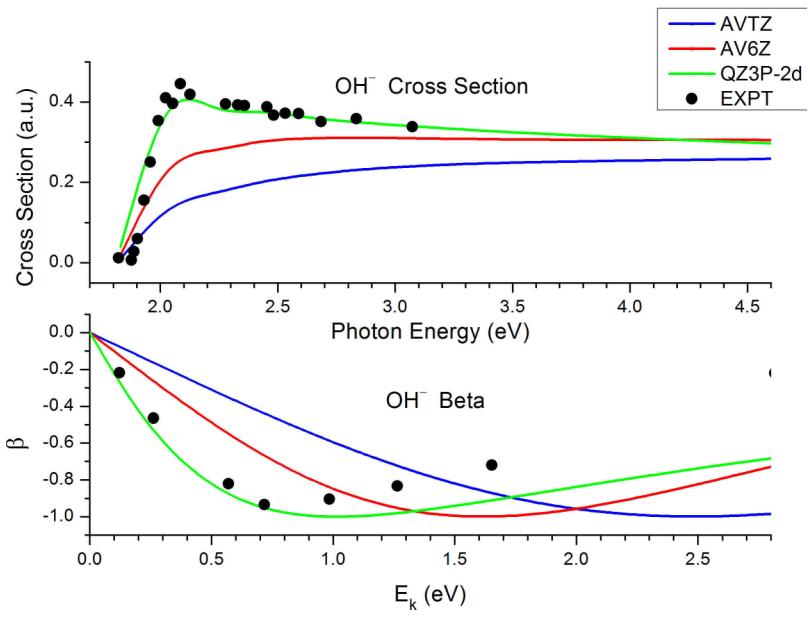

FIG. 5. Calculated photodetachment cross section (upper panel) and anisotropy parameter β (lower panel) of OH^- anion with AVTZ (in blue), AV6Z (in red), and STO QZ3P-2d (in green) basis sets. The experimental data (black circle) are from Refs. 59 and 70.

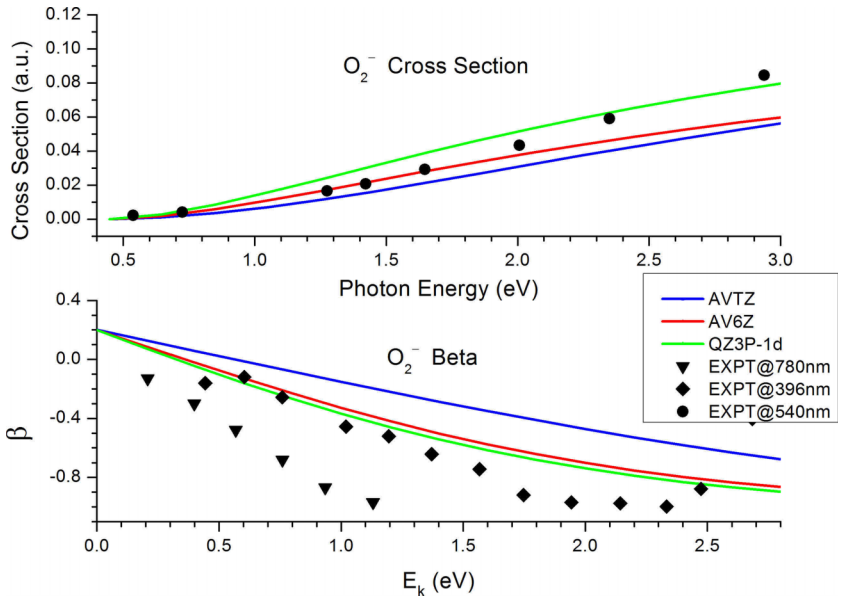

FIG. 6. Calculated photodetachment cross section (upper panel) and anisotropy parameter β (lower panel) of O_2^- anion with AVTZ (in blue), AV6Z (in red), and STO QZ3P-1d (in green) basis sets. The experimental data (black circle, triangle, and diamond) are from Refs. 71 and 72.

OH^- anion and O_2^- anion, respectively. In Fig. 5, as we have seen before, the two GTO basis sets (blue line and red line) slightly underestimate the cross section. As the photon energy is above the photodetachment threshold, there is a steep rise in the experimental photodetachment cross section, and after it reaches its maximum, it gradually drops. The calculation using GTOs predicted a gradual slope, and then it becomes flat, not consistent with the experimental observation. However, the calculation using STO basis sets QZ3P-2d overcomes the problems and is in excellent agreement with the experimental results. For β value, similar to the case in Fig. 3 for O^- anion, GTOs tend to give slower changes compared to the experimental results even with AV6Z. In the lower panel of Fig. 5, the STO QZ3P-2d gives a better performance than all GTOs. Specially in lower kinetic energy region, it reproduces the experimental β very well. In Fig. 6 (upper panel), both calculations using STO QZ3P-1d basis sets and GTOs are in good agreement with the experimental results at 540 nm laser radiation (2.30 eV, black circle) for cross sections. In the lower pane of Fig. 6, the calculations slightly overestimate β values. For the photon energy 780 nm (1.59 eV, black triangle), only the state $X^3\Sigma_g^-$ of neutral O_2 is reached, which is the state we calculated. While at 396 nm (3.13 eV, black diamond), the overlapped transitions from O_2^- anion $X^2\Pi_g$ to O_2 neutral $X^3\Sigma_g^-$, $a^1\Delta_g$, and $b^1\Sigma_g^+$ occur, which were not taken into account in the calculations.

Fig. 7 shows the comparison between the calculations and the experimental results for NH_2^- anion. The experimental cross section is in a relative scale, so a scaling factor is used for comparison with the theoretical calculations for the best fitting. All GTOs and STOs produced the slower rises of cross sections when compared to the experimental slope. All three basis sets well reproduce the anisotropy parameter β. Interestingly, the β values given by our method here are very close to the prediction by the mixed s-p states model.[14]

In Fig. 8, the anisotropy parameter β values using different basis sets are presented for CH^- anion (upper panel) and S_2^- anion (lower panel). The experimental data of their cross

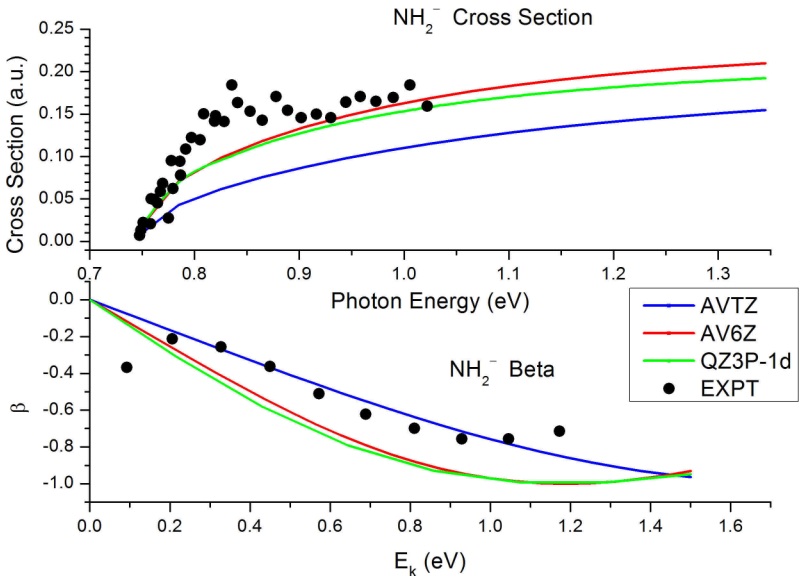

FIG. 7. Calculated photodetachment cross section (upper panel) and anisotropy parameter β (lower panel) of NH_2^- anion with AVTZ (in blue), AV6Z (in red), and STO QZ3P-1d (in green) basis sets. The experimental data (black circle) are from Refs. 11 and 60.

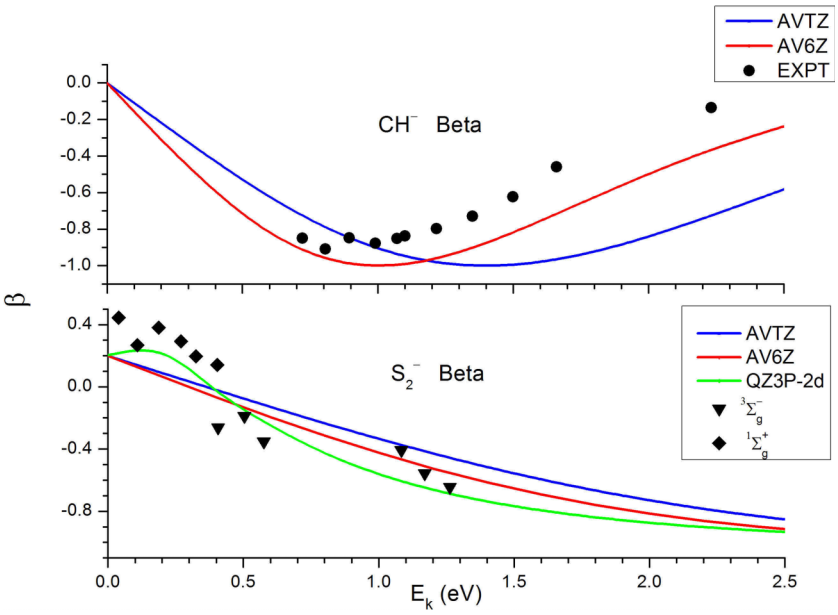

FIG. 8. Calculated anisotropy parameter β of CH^- anion (upper panel) and S_2^- anion (lower panel) with AVTZ (in blue), AV6Z (in red), and STO QZ3P-2d (in green) basis sets. The experimental data (black circle, triangle, and diamond) are Refs. 74 and 73.

section are absent in the literature. For CH^-, the calculations slightly underestimate β in the high kinetic energy region, and the larger basis sets AV6Z present a better performance than AVTZ. Basically, S_2^- anion has the same valence structure as O_2^- anion. There are three transition channels corresponding to the neutral states $^3\Sigma_g^-$, $^1\Delta_g$, and $^1\Sigma_g^+$ of S_2. The $^3\Sigma_g^-$ and $^1\Sigma_g^+$ are the results of photodetachment from the π_g orbital. The calculations using GTOs and STOs reproduce β values of both channels very well. The β values predicted by the present work for S_2^- are closer to the experimental values than both the Dyson orbital model[30] and the Cooper-Zare model.[73]

It should be noted that HOMOs of O_2^- and S_2^- are degenerate π_g^* orbitals, which resemble atomic d orbitals. According to the simplified Cooper-Zare equation by Hanstorp *et al.*,[13] for an atomic d orbital, β value should be exactly 0.2 at threshold energy. Indeed, our analytical spherical-average method reproduces β = 0.2 at threshold.

Generally, the calculations of photodetachment cross sections and anisotropy parameters β depend heavily on the size of basis sets, which is probably due to the diffuse nature of anions' wave functions. Even with the AV5Z (data not shown here) and AV6Z Dunning's correlation basis sets, it seems that the calculations still do not approach the basis set limit. The present investigation shows that STOs usually reproduce experimental results better than GTOs. This might be due to the different asymptotic behaviors of GTOs and STOs. The form of the dipole operator $\vec{\varepsilon} \cdot \vec{r}$ means that the charge density at the large distance has greater weight. As $r \to \infty$, the asymptotic behavior of GTO is $e^{-\alpha r^2}$, while $e^{-\xi r}$ for STO. The latter asymptotic behavior is correct for real anions.

V. CONCLUSIONS

The DFT Kohn-Sham orbitals are used to calculate the photodetachment cross section and anisotropy parameter β of anions. Present work shows that the calculations based on DFT Kohn-Sham orbitals can well reproduce the experimental photodetachment cross sections and anisotropy parameters β of Li^-, C^-, O^-, F^-, CH^-, OH^-, NH_2^-, O_2^-, and S_2^-, and the performance of STO basis sets is better than that of GTO.

It should be pointed out that, compared with many-body theories, DFT calculations do not account for orbital relaxation effects. If the relaxation effects are significant after photodetachment, DFT may not work well. One example is the photodetachment from H^-, a prototype for quantum three-body problems. DFT cannot well reproduce the experimental results of photodetachment from H^-. Generally, many-body theories can treat the electron correlation effects more accurately than DFT does, and Dyson orbitals based on a many-body theory take into consideration the orbital relaxation effects but DFT Kohn-Sham orbitals do not. The performance of high-level many-body theories can be improved in a systemic way, but no such a way for DFT. Therefore, if a very accurate calculation is required, a high-level many-body theory with STO basis sets may be a promising alternative.

The advantage of the present DFT method is more efficient and easier to use. The diffusion nature of anions' wave function usually demands large basis sets, which may make the computational cost unbearable using high level many-body theories for a larger system. Therefore, the present method provides an efficient way to calculate the photodetachment cross section and the anisotropy parameter β for large systems.

ACKNOWLEDGMENTS

This work is supported by National Natural Science Foundation of China (NSFC) (Grant Nos. 11174175 and 91336104) and Ministry of Science and Technology of China (MOST) (Grant No. 2013CB922004) of the National Key Basic Research Program of China.

[1]A. Eppink and D. H. Parker, Rev. Sci. Instrum. **68**, 3477 (1997).
[2]I. Leon, Z. Yang, H. T. Liu, and L. S. Wang, Rev. Sci. Instrum. **85**, 083106 (2014).
[3]E. Surber and A. Sanov, J. Chem. Phys. **116**, 5921 (2002).
[4]D. M. Neumark, J. Phys. Chem. A **112**, 13287 (2008).

[5]A. Osterwalder, M. J. Nee, J. Zhou, and D. M. Neumark, J. Chem. Phys. **121**, 6317 (2004).
[6]H. T. Liu, C. G. Ning, D. L. Huang, P. D. Dau, and L. S. Wang, Angew. Chem., Int. Ed. **52**, 8976 (2013).
[7]C. G. Ning, P. D. Dau, and L. S. Wang, Phys. Rev. Lett. **105**, 263001 (2010).
[8]M. L. Weichman, J. B. Kim, J. A. DeVine, D. S. Levine, and D. M. Neumark, J. Am. Chem. Soc. **137**, 1420 (2015).
[9]T. Westermann, J. B. Kim, M. L. Weichman, C. Hock, T. I. Yacovitch, J. Palma, D. M. Neumark, and U. Manthe, Angew. Chem., Int. Ed. **53**, 1122 (2014).
[10]X. P. Xing, X. B. Wang, and L. S. Wang, Phys. Rev. Lett. **101**, 083003 (2008).
[11]A. Sanov, E. R. Grumbling, D. J. Goebbert, and L. M. Culberson, J. Chem. Phys. **138**, 054311 (2013).
[12]A. Sanov, Annu. Rev. Phys. Chem. **65**, 341 (2014).
[13]D. Hanstorp, C. Bengtsson, and D. J. Larson, Phys. Rev. A **40**, 670 (1989).
[14]E. R. Grumbling and A. Sanov, J. Chem. Phys. **135**, 164302 (2011).
[15]J. Cooper and R. N. Zare, J. Chem. Phys. **49**, 4252 (1968).
[16]J. Cooper and R. N. Zare, J. Chem. Phys. **48**, 942 (1968).
[17]J. C. Tully, R. S. Berry, and B. J. Dalton, Phys. Rev. **176**, 95 (1968).
[18]A. Sanov and R. Mabbs, Int. Rev. Phys. Chem. **27**, 53 (2008).
[19]K. L. Reid, Annu. Rev. Phys. Chem. **54**, 397 (2003).
[20]T. Seideman, Annu. Rev. Phys. Chem. **53**, 41 (2002).
[21]C. N. Yang, Phys. Rev. **74**, 764 (1948).
[22]E. P. Wigner, Phys. Rev. **73**, 1002 (1948).
[23]H. A. Bethe and E. E. Salpeter, *Quantum Mechanics of One- and Two-Electron Atoms* (Plenum, New York, 1977).
[24]L. M. Culberson, C. C. Blackstone, and A. Sanov, J. Phys. Chem. A **117**, 11760 (2013).
[25]E. R. Grumbling and A. Sanov, J. Chem. Phys. **135**, 164301 (2011).
[26]A. Humeniuk, M. Wohlgemuth, T. Suzuki, and R. Mitric, J. Chem. Phys. **139**, 134104 (2013).
[27]H. Koch, R. Kobayashi, A. S. Demeras, and P. Jorgensen, J. Chem. Phys. **100**, 4393 (1994).
[28]J. F. Stanton and R. J. Bartlett, J. Chem. Phys. **98**, 7029 (1993).
[29]H. Koch and P. Jorgensen, J. Chem. Phys. **93**, 3333 (1990).
[30]C. M. Oana and A. I. Krylov, J. Chem. Phys. **131**, 124114 (2009).
[31]C. M. Oana and A. I. Krylov, J. Chem. Phys. **127**, 234106 (2007).
[32]P. Duffy, D. P. Chong, M. E. Casida, and D. R. Salahub, Phys. Rev. A **50**, 4707 (1994).
[33]W. Kohn and L. J. Sham, Phys. Rev. **140**, A1133 (1965).
[34]Y. Liu, L. F. Cheung, and C. G. Ning, Chin. Phys. B **23**, 063403 (2014).
[35]Y. R. Miao, C. G. Ning, and J. K. Deng, Phys. Rev. A **83**, 062706 (2011).
[36]Y. R. Miao, C. G. Ning, K. Liu, and J. K. Deng, J. Chem. Phys. **134**, 204304 (2011).
[37]C. G. Ning, B. Hajgato, Y. R. Huang, S. F. Zhang, K. Liu, Z. H. Luo, S. Knippenberg, J. K. Deng, and M. S. Deleuze, Chem. Phys. **343**, 19 (2008).
[38]F. O. Ellison, J. Chem. Phys. **61**, 507 (1974).
[39]K. J. Reed, A. H. Zimmerman, H. C. Andersen, and J. I. Brauman, J. Chem. Phys. **64**, 1368 (1976).
[40]M. E. Rose, *Elementary Theory of Angular Momentum* (John Wiley & Sons, New York, 1957).
[41]A. D. Becke, J. Chem. Phys. **98**, 5648 (1993).
[42]B. Miehlich, A. Savin, H. Stoll, and H. Preuss, Chem. Phys. Lett. **157**, 200 (1989).
[43]L. Chengteh, Y. Weitao, and R. G. Parr, Phys. Rev. B **37**, 785 (1988).
[44]See http://www.gaussian.com for Gaussian program (Gaussian, Inc., Wallingford CT, 2004).
[45]See http://www.scm.com for ADF Program (SCM, Amsterdam).
[46]T. H. Dunning, J. Chem. Phys. **90**, 1007 (1989).
[47]E. Weigold and I. E. McCarthy, *Electron Momentum Spectroscopy* (Kulwer Academic, New York, 1999).
[48]M. A. Coplan, J. H. Moore, and J. P. Doering, Rev. Mod. Phys. **66**, 985 (1994).
[49]C. G. Ning, S. F. Zhang, J. K. Deng, K. Liu, Y. R. Huang, and Z. H. Luo, Chin. Phys. B **17**, 1729 (2008).
[50]X. G. Ren, C. G. Ning, J. K. Deng, S. F. Zhang, G. L. Su, F. Huang, and G. Q. Li, Rev. Sci. Instrum. **76**, 063103 (2005).
[51]H. Nakatsuji, Chem. Phys. Lett. **67**, 329 (1979).
[52]G. Haeffler, D. Hanstorp, I. Kiyan, A. E. Klinkmuller, U. Ljungblad, and D. J. Pegg, Phys. Rev. A **53**, 4127 (1996).
[53]J. Dellwo, Y. Liu, D. J. Pegg, and G. D. Alton, Phys. Rev. A **45**, 1544 (1992).
[54]M. Scheer, R. C. Bilodeau, C. A. Brodie, and H. K. Haugen, Phys. Rev. A **58**, 2844 (1998).
[55]C. Valli, C. Blondel, and C. Delsart, Phys. Rev. A **59**, 3809 (1999).
[56]C. Blondel, C. Delsart, and F. Goldfarb, J. Phys. B: At., Mol. Opt. Phys. **34**, L281 (2001).
[57]C. Blondel, P. Cacciani, C. Delsart, and R. Trainham, Phys. Rev. A **40**, 3698 (1989).
[58]A. Kasdan, E. Herbst, and W. C. Lineberger, Chem. Phys. Lett. **31**, 78 (1975).
[59]L. M. Branscomb, Phys. Rev. **148**, 11 (1966).
[60]K. C. Smyth and J. I. Brauman, J. Chem. Phys. **56**, 4620 (1972).
[61]K. M. Ervin, W. Anusiewicz, P. Skurski, J. Simons, and W. C. Lineberger, J. Phys. Chem. A **107**, 8521 (2003).
[62]S. Moran and G. B. Ellison, J. Phys. Chem. **92**, 1794 (1988).
[63]A. M. Covington, D. Calabrese, W. W. Williams, J. S. Thompson, and T. J. Kvale, Phys. Rev. A **56**, 4746 (1997).
[64]M. L. Seman and L. M. Branscomb, Phys. Rev. **125**, 1602 (1962).
[65]L. M. Branscomb, S. J. Smith, and G. Tisone, J. Chem. Phys. **43**, 2906 (1965).
[66]S. J. Cavanagh, S. T. Gibson, and B. R. Lewis, J. Phys.: Conf. Ser. **212**, 012034 (2010).
[67]A. Mandl, Phys. Rev. A **3**, 251 (1971).
[68]S. Vacquie, A. Gleizes, and M. Sabsabi, Phys. Rev. A **35**, 1615 (1987).
[69]H. J. Kaiser, E. Heinicke, R. Rackwitz, and D. Feldmann, Z. Phys. **270**, 259 (1974).
[70]G. Aravind, A. K. Gupta, M. Krishnamurthy, and E. Krishnakumar, Phys. Rev. A **76**, 042714 (2007).
[71]D. S. Burch, S. J. Smith, and L. M. Branscomb, Phys. Rev. **112**, 171 (1958).
[72]F. A. Akin, L. K. Schirra, and A. Sanov, J. Phys. Chem. A **110**, 8031 (2006).
[73]E. Surber, R. Mabbs, and A. Sanov, J. Phys. Chem. A **107**, 8215 (2003).
[74]B. Bandyopadhyay, C. J. M. Pruitt, and D. J. Goebbert, J. Chem. Phys. **138**, 201101 (2013).